Pergamon

Geochimica et Cosmochimica Acta, Vol. 68, No. 4, pp. 729–741, 2004

0016-7037/04 $30.00 + .00

doi:10.1016/S0016-7037(03)00489-7

Molecular characterization of cyanobacterial silicification using synchrotron infrared micro-spectroscopy

LIANE G. BENNING,[1,*] V. R. PHOENIX,[2] N. YEE,[1] and M. J. TOBIN[3]

[1]School of Earth Sciences, University of Leeds, Leeds, LS2 9JT, UK
[2]Department of Geology, University of Toronto, Toronto, ON M5S 3B1, Canada
[3]Synchrotron Radiation Department, CLRC, Daresbury Laboratory, Warrington, WA4 4AD, UK

(*Received August* 6, 2002; *accepted in revised form April* 21, 2003)

Abstract—Synchrotron-based Fourier-transform infrared (SR-FTIR) micro-spectroscopy was used to determine the concentration-dependent response of the organic structure of live cyanobacterial cells to silicification. Mid-infrared (4000–600 cm^{-1}) measurements carried out on single filaments and sheaths of the cyanobacteria *Calothrix* sp. (strain KC97) were used to monitor the interaction between a polymerizing silica solution and the organic functional groups of the cells during progressive silicification. Spectra of whole-cells and sheaths were analyzed and the spectral features were assigned to specific functional groups related to the cell: lipids (-CH_2 and -CH_3; at 2870–2960 cm^{-1}), fatty acids (>C=O at 1740 cm^{-1}), proteins (amides I and II at 1650 and 1540 cm^{-1}), nucleic acids (>P=O 1240 cm^{-1}), carboxylic acids (C-O at 1392 cm^{-1}), and polysaccharides (C-O between 1165 and 1030 cm^{-1}). These vibrations and the characteristic vibrations for silica (Si-O between 1190 and 1060 cm^{-1}; to some extent overlapping with the C-O frequencies of polysaccharides and Si-O at 800 cm^{-1}) were used to follow the progress of silicification. Relative to unsilicified samples, the intensity of the combined C-O/Si-O vibration band increased considerably over the course of the silicification (whole-cells by > 90% and sheath by ~75%). This increase is a consequence of (1) extensive growth of the sheath in response to the silicification, and (2) the formation of thin amorphous silica layers on the sheath. The formation of a silica specific band (~800 cm^{-1}) indicates, however, that the precipitation of amorphous silica is controlled by the dehydroxylation of abiotically formed silanol groups. *Copyright © 2004 Elsevier Ltd*

1. INTRODUCTION

Cyanobacteria are a major group of oxygenic, phototrophic prokaryotes, often found in hot spring environments (Fay, 1983; Ward et al., 1998; Brock et al., 1994), where it has been proposed that they participate in both metabolically induced and passive mineral formation reactions (Lowenstam, 1981; Krumbein, 1983; Fortin et al., 1997). Although the active precipitation of amorphous silica (opal A) is one of the most obvious and important geological processes in many modern hot springs, the role microorganisms play in the precipitation process is unclear. In modern settings, during ascent to the Earth's surface and upon exposure to atmospheric conditions, geothermal waters undergo extreme changes in chemical (e.g., redox, pH, saturation state) and physical (e.g., temperature, pressure) properties (Henley et al., 1984). These changes induce the precipitation of amorphous silica (and other components) and this affects the chemical environment of the microbial communities that live in the subboiling parts of thermal springs. In such environments, the supply of aqueous silica in the effluent solution is continuous and often supersaturated with respect to amorphous silica and silica adsorption/precipitation processes can be sustained via inorganic processes. The kinetic and thermodynamic parameters controlling inorganic silica precipitation and stability have been quantified in a series of field and laboratory studies (e.g., Rimstidt and Barnes, 1980; Fournier, 1985; Dove and Crerar, 1990; Carroll et al., 1998). Furthermore, experimental studies with pure cell cultures have shown that microbial surfaces have a low affinity for silica when compared with metals (Ferris et al., 1988; Daughney et al., 1998; Phoenix, 2001; Fein et al., 2002; Phoenix et al., submitted; Yee et al., in press). However, ample circumstantial laboratory and field-based evidence suggests that the presence of microorganisms may influence the precipitation of amorphous silica from modern hot spring fluids (e.g., Walter et al., 1972; Ferris et al., 1986; Schultze-Lam et al., 1995; Westall et al., 1995; Konhauser and Ferris, 1996; Jones et al., 2000; Phoenix et al., 2000; Konhauser et al., 2001; Mountain et al., 2002). It has been speculated that microorganisms might act as possible nucleation sites for aqueous silica, thus influencing silica polymerization rates. Yet, direct evidence for an active role of microbial cells in the silicification process is so far lacking.

Many geochemical reactions may be affected by microbial metabolism in geothermal environments, but interactions between microbial cells and the geothermal solutions are still poorly understood. This is mainly a consequence of the dearth of in situ and in vivo experimental data quantifying microbe-mineral and microbe-fluid interactions. The molecular level quantification of the interaction between a polymerizing silica solution and the cell surface functional components remains the critical step in elucidating silicification processes occurring in near-Earth surface geothermal systems. Only such studies can provide data for a mechanistic model, which may be applied to a whole range of biomineralization reactions. Furthermore, understanding the interactions that occur at the microbe/fluid/mineral interface in modern geothermal settings, will improve the ability to interpret some of the earliest records of life on Earth (e.g., Archean siliceous stromatolites and their recogniz-

* Author to whom correspondence should be addressed (l.benning@earth.leeds.ac.uk).

able microfossils, Awramik, 1992; Cady, 2001), which provide a proxy for the biogeochemical conditions of the early biosphere. Batch-type measurements can reveal changes in bulk concentrations of inorganic or organic species in microbial microcosms. However, the lack of temporal and spatial control in such studies precludes detailed measurements of mineral/fluid/interactions. Conversely, in situ experiments, can provide quantitative data on the effective changes in reactions occurring at the microbe/fluid/mineral interface and this can be done time resolved and in vivo.

In this study, results from microbe/fluid/mineral interaction experiments that were followed in situ and in vivo are presented. The experiments were carried out with cultured cyanobacterial filaments and the changes in the chemistry of their organic framework and their response to precipitation of amorphous silica was ascertained. The main questions that have been addressed are: (1) what role do cyanobacteria play in the biomineralization process and (2) how do cyanobacterial cells respond to changes in the chemical environment they live in? The results show that it is possible to establish the vibrational frequencies, which correspond to the organic functional groups of cyanobacterial cells and cell components, and to ascertain and quantify the changes in cell composition in response to silicification.

2. BACKGROUND: FOURIER TRANSFORM INFRARED MICRO-SPECTROSCOPY AND MICROORGANISMS

Fourier transform infrared (FTIR) spectroscopy has proven to be a fundamental technique that can provide an unique and accurate insight into the in situ and in vivo changes in the chemical character of human and microbial cells at high spatial resolution. For biologic spectroscopy, the important vibrations occur in the mid-infrared region (700–4000 cm^{-1} or wavelengths, λ, between 2.5 and 16 μm) where most organic molecules show characteristic spectral features (Diem, 1993, Naumann et al., 1996). Infrared light is absorbed when the vibrational motion (e.g., stretching, bending, and rotating) of a species (e.g., a molecule, functional group, or cation-anion pair) induces a change in its dipole moment. The strength and frequency of infrared absorptions are determined primarily by factors that include symmetry, bond type and the masses of the atoms (McMillan and Hofmeister, 1988; Diem, 1993; Stuart and Ando, 1997).

2.1. Conventional FTIR and Micro-Spectroscopy

In the last few decades, conventional thermal FTIR spectroscopy has been extensively used in biology and medicine (1) to characterize cell compounds and structures (Parker, 1983; Naumann et al., 1991; Diem, 1993) (2) to differentiate, classify, and identify microorganisms (Naumann et al., 1996; Naumann, 2000; Choo-Smith et al., 2001) and (3) to detect, enumerate, and identify microcolonies (Schultz and Naumann, 1991; Diem et al., 1999). Furthermore, FTIR measurements may be carried out on untreated (e.g., unstained) material, thus preserving the integrity of the original cells. The combination of infrared spectroscopy with microscopy (thermal FTIR micro-spectroscopy) has improved the spectral quality and reproducibility of infrared measurements of small samples (Wetzel and LeVine, 1999; Lasch et al., 2002). Thermal FTIR-micro-spectroscopy on biologic samples was pioneered in the medical sciences where it is used as a clinical tool to distinguish between malignant and healthy human cells (i.e., to quantify the development of cancer, Alzheimer's disease or bone osteoporosis, Naumann, 1997; LeVine and Wetzel, 1998; Chiriboga et al., 2000). To date only a few studies have used conventional thermal FTIR micro-spectroscopy to characterize the organic composition of natural environmental samples or their effect on geochemical and biochemical cycles. Usually such studies have been carried out with mixed-cultures and were used as a discriminatory tool (Schuster et al., 1999; Naumann, 2000; Choo-Smith et al., 2001) or to follow bulk reactions in biotechnological processes (Kansiz et al., 1999; Giordano et al., 2001).

Thermal FTIR is usually used to characterize bulk samples, and in the midinfrared, the microscope incident beam can typically be focussed to an area of $\sim 100 \times 100\ \mu m^2$. However, a further increase in spatial resolution can only be achieved by the use of slits or apertures and this results in a dramatic decrease in signal to noise ratio for a given scan time.

2.2. Synchrotron-Based FTIR-Micro-Spectroscopy (SR-FTIR)

The most exciting advance in the field of FTIR-micro-spectroscopy has occurred with the implementation of synchrotron-based FTIR micro-spectroscopy (SR-FTIR; Fig. 1). This technique has only recently been used to image changes in the molecular characteristics of cells during the growth and life cycles of isolates or mixed cultures (Jamin et al., 1998a, 1998b; Miller et al., 1998, 2002; Tobin et al., 1999; Holman et al., 2000b). Depending on the specific biochemical character of a species or strain, SR-FTIR micro-spectroscopy has been used: (1) to track changes in the organic structure of live cells (Jamin et al., 1998a, Holman et al., 2000b); (2) to follow the development of environmentally induced changes in the overall molecular framework of cells (Holman et al., 1999, 2000a, 2002; Benning et al., 2002) and (3) to distinguish and discriminate changes in specific biogeochemical environments (Sigee et al., 2002).

Synchrotron-based FTIR micro-spectroscopy has clear advantages over thermal-based FTIR micro-spectroscopy due to the 100 to 1000 times greater brightness (higher photon flux; Carr, 1999). However, this improvement is not due to a higher emitted power but, because the effective source size is smaller and the light is emitted into a narrower range of angles. The relationship between the emitted power and the source area allows smaller regions to be probed and for a 10-μm aperture, a $>$ 1000 times better signal to noise ratio is observed for the synchrotron source compared with a thermal source (Reffner et al., 1995; Martin et al., 2002). Furthermore, this also results in a 10-fold improvement on spatial resolution (Carr, 2001). SR-FTIR micro-spectroscopy permits measurements of the organic structure of individual microorganisms and their environment non-destructively and rapidly (seconds to tens of seconds). Due to the non-destructive nature of infrared light, microorganisms can be observed in situ and in vivo and the changes in their biochemical character can be monitored over time and with changing solution composition. Since there is no need for sample preparation (no fixation, staining, etc.) the organic

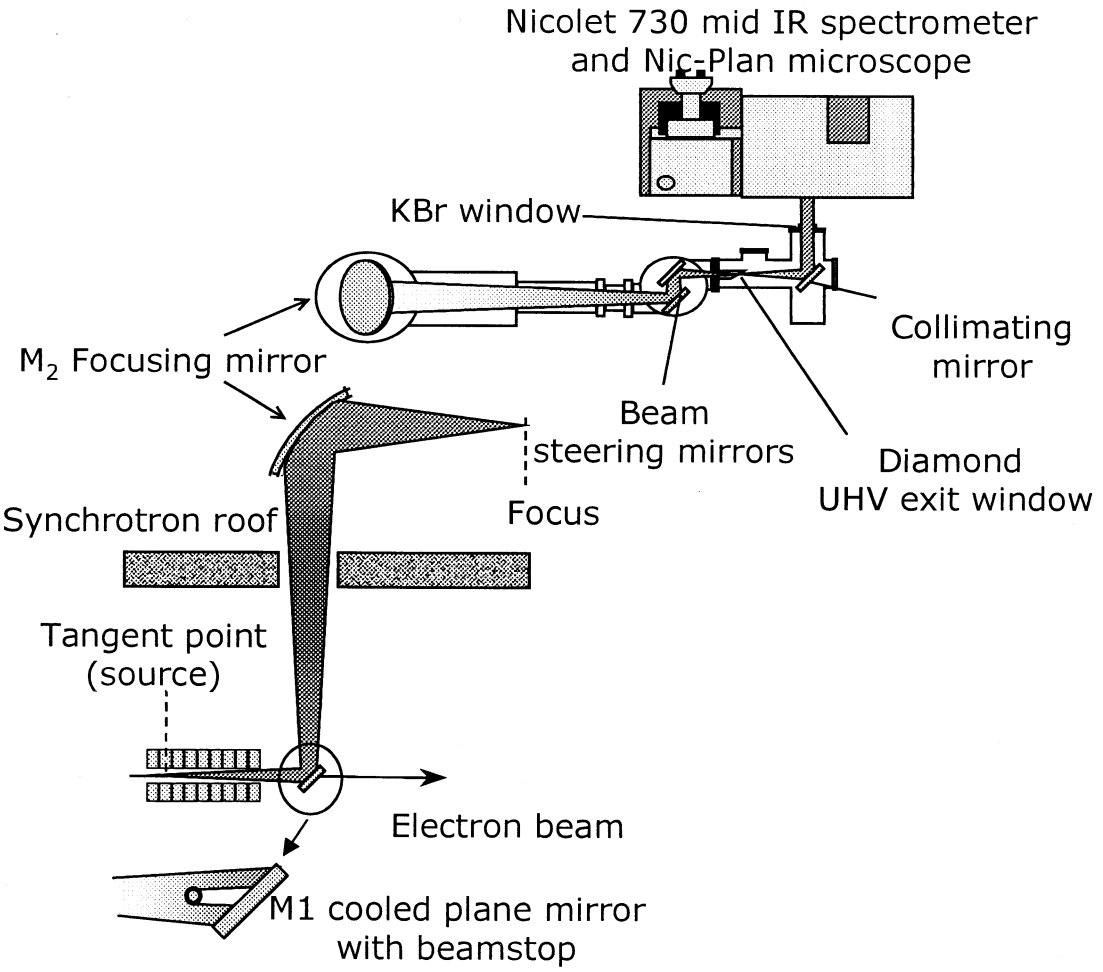

Fig. 1. Schematic of infrared micro-spectroscopic set-up at beam line 13.3 at the Daresbury Laboratory. Additional details of the beamline and its performance are given in Tobin et al. (1999).

functional character of biomolecules is retained. With infrared light radiation damage is not observed even for counting times up to 30 min (Martin et al., 2001).

In this study, SR-FTIR micro-spectroscopy was used to study single cyanobacterial filaments and their response to changes in their chemical environment. These changes were monitored in situ and in vivo via the variations in mid-infrared band intensity and position. Such variations were linked to several factors, including increasing concentration of an absorbed surface species or variations in density of various cellular components.

2.3. Organic Components of Cyanobacterial Cells

Microbial cells consist of complex chemical macromolecules that are distributed in various cellular components. They include the cytoplasm (dominated by proteins and nucleic acids), the cytoplasmic cell membrane (composed predominantly of phospholipids), and the cell wall (composed predominantly of peptidoglycan). The cell walls of gram-negative Bacteria (such as the strain used here, *Calothrix* sp.) also contain an outer membrane (mainly composed of phospholipids and lipopolysaccharides). In the case of *Calothrix* sp. the cell wall is surrounded by a sheath composed of a complex array of polysaccharides (e.g., Weckesser et al., 1988). The cyanobacterial sheath separates the cell from its surrounding environment and act as a shield against dehydration and predation, or protects the cell wall from detrimental metal uptake or biomineralization (Dudman, 1977; Weckesser et al., 1988; Scott et al., 1996; Hoiczyk, 1998; Wilson et al., 2001; Phoenix et al., 2002).

On average, the composition of Bacterial cells are fairly homogeneous: ~40 to 60% proteins, ~15 to 20% nucleic acids, ~10 to 15% polysaccharides, ~10 to 15% lipids, and ~1 to 3% other organic and inorganic components (e.g., Brock et al., 1994, Naumann, 2000). Naturally, this composition depends on a variety of factors including cell division stage and growth cycle. It was assumed that the average composition noted above applied to the whole-cells of the culture used in these experiments (see below). In the cytoplasm, the proteins dominate the vibrational spectra because the total concentration of proteins is high (~100 mmol/L, Diem et al., 1999). Although, the average infrared spectra of all proteins are remarkably constant, the intensity and frequencies for proteins may

vary depending on their primary and secondary structure, their hydration state, as well as the ionic strength of the solvent. In cyanobacteria, the content of polysaccharides can be significantly higher due to the presence of an extracelluar polysaccharide sheath which may represent up to 20 to 30% of dry mass of the whole-cell (Weckesser et al., 1988).

The sheath of the cyanobacteria that was studied here (*Calothrix* sp.) consists of ~50% neutral sugars, mainly glucose, and ~5% amino acids (of sheath dry weight; Drews and Weckesser, 1982; Weckesser et al., 1988). Often sugars are also found in the cell body but then they are combined with proteins and form glycoproteins. The hydration state of a cell is strongly dependent on the hydration of this sugar "coating" and this will strongly affect the infrared vibrations because in most microbial cells the enzymatic changes are controlled by the changes in protonation states of the functional groups.

3. MATERIALS AND METHODS

3.1. Microbial Culture, Silicification Experiments and Reference Materials

The silicification experiments were carried out with the filamentous cyanobacteria *Calothrix* sp. (strain KC97, Phoenix et al., 2000). Cultures were obtained by growth for 4 weeks in autoclaved liquid BG11-N media at 28°C, under cool florescent light at an intensity of 25 μmol m^{-2} s^{-1}. Four-week-old cultures were used, as *Calothrix* sp. is a relatively slow growing organism that takes weeks to produce a suitable dense culture for experimentation. After 4 weeks growth, the colonies were healthy and in growth phase. Once such a suitable culture was obtained, a series of microcosms, each one with a biomass of 2.3 mg dry weight (see below), were prepared in 50-mL polypropylene centrifuge tubes. Standard 10.7 mmol/L (300 ppm) monomeric Si solutions were prepared from $Na_2SiO_3 \cdot 7H_2O$ and sterile 18 MΩ water. Polymerization of this solution was induced just before addition to each microcosm by neutralizing to pH ~ 7 with 2 mol/L HCl. Immediately thereafter, silicification experiments were initiated by adding to each microcosm 10 mL of the freshly neutralized 10.7 mmol/L Si solution containing 10% BG11-N. The silicification process was sustained by exchanging the Si solution every 2 to 3 days with fresh Si solution for a maximum of 12 times. In a parallel study (Phoenix, 2001), for each exchange step an average of 3.6 μmol Si were estimated to be sorbed by the cyanobacterial biomass (2.3 mg/microcosm; Phoenix, 2001). Therefore, after 12 exchanges a maximum of ~43 μmol Si was sorbed onto the cell surface. Silica sorption was determined by measuring the amount of silica remaining in solution (via ICP-AES). The amount sorbed onto the reaction vessel wall was determined from a control (cyanobacteria free) experiment. Thus, the total silica sorbed by the cyanobacteria was calculated as the difference between that immobilized in the control and that immobilized in the cyanobacterial microcosm (Phoenix, 2001).

Unsilicified *Calothrix* sp. whole-cells (i.e., intact chains of cells enclosed within a polysaccharide sheath) and unsilicified chemically purified *Calothrix* sp. sheaths (see below) were used as controls. These two microbial control fractions together with the standard 10.7 mmol/L silica solution were used as reference materials for identification and verification of band assignments. Chemically purified *Calothrix* sp. sheaths were obtained via a method modified after Weckesser et al. (1988). Mature cultures were homogenized in a tissue grinder, followed by 6 h ultrasonication in a Branson 3200 sonicating bath. The homogenates were washed by centrifugation at 3000*g* re-suspended in 100 mL of 0.05 mol/L HEPES buffer (pH 6.8) with 200 mg/L lysozyme (chicken egg white; EC. 3.2.1.17), and incubated for 16 h at 37°C. After incubation, the resulting fraction was added drop wise to 100 mL of boiling 4% *w*/*v* (final concentration = 2%*w*/*v*) sodium dodecyl sulfate (SDS). After boiling for 15 min, the remaining purified sheath fractions were washed 7 times in 18 MΩ water by centrifugation at 20,000*g*.

3.2. Infrared Measurements and Data Analysis

3.2.1. Sample and Reference Material Preparation

Just before the infrared measurements, aliquots of each microcosm were diluted and washed three times in 50 mL of 18 MΩ water with intermittent centrifugation at 5000*g* to remove all the organic components associated with the BG11-N media and the non-bound silica (both monomeric and polymeric fractions). To disperse the filamentous clusters, the washed pellets were transferred to a 1.5-mL Eppendorf tube and sonicated for three 10-s cycles using an ultrasconic disintegrator (Sanyo Soniprep 150) with an output frequency of 23 kHz and 6-μm amplitude. Immediately after sonication, 100 ± 2 μL of each sample suspension were placed onto low-emissivity infrared reflectance slides (Kevley Technologies, USA), which show a 100% reflectance across the mid-IR. The slides were dried in an incubator at 30°C for 4 h. In addition, samples of each reference material (unsilicified whole-cell control, unsilicified chemically purified sheath control and the 10.7 mmol/L silica standard solution) were prepared in the same way. During sonication, of the whole-cell materials (both reference and silicified) most filaments remained intact. However, some of the sheaths were mechanical partially separated from the silicified filaments (Fig. 2), and in all discussions below, spectra of silicified whole-cells (including sheath, section 4.2.1.) or spectra of separated silicified sheaths (described in section 4.2.2.) refer to analyses performed on these two fractions. Note that the silicification was not carried out on chemically purified sheaths, but that the separated sheaths discussed below were silicified on the original filaments and than mechanically separated during sonication. This is different to the chemically purified sheaths, which were used as sheath control for spectral assignments and which were not silicified (see above). Previous work has shown that the synchrotron infrared light is not damaging to microbial cells (Martin et al., 2001). During a later examination of the silicified samples (repeat spectra collected on same samples), strong water peaks were still visible in all cell spectra, suggesting that full dehydration of the cells had not occurred. Furthermore, although we did not carry out viability counts after analysis, the successful culturing of cyanobacteria from the slides corroborated the that cells were still viable post-analysis.

3.2.2. Spectrometer and Microscope Set-up

The infrared measurements were carried out on station 13.3 at the Daresbury Laboratory, Warrington (UK) using a Nicolet NicPlan Infrared Microscope fitted with a 730 mid-IR spectrometer with the light derived from an external synchrotron source (Fig. 1; Tobin et al., 1999). The spectra were collected in reflectance mode with a liquid N_2 cooled mercury-cadmium-telluride (MCT) detector, at a resolution of 8 cm^{-1} by co-adding 256 scans per point. A Happ-Genzel apodisation function was used, with the zero-filling factor set to two. In this mode, the infrared beam passes through the sample, is reflected off the IR slide (100% reflecting), and is collected with the microscope operating in reflectance mode. The synchrotron beam on station 13.3 focuses, unapertured, to ~20 × 30 μm^2, and with the slits set to 20 × 10 μm^2, the full intensity of the beam is not used, thus avoiding saturation automatically. Nevertheless, the interferograms corresponding to the background and to the sample were carefully checked for saturation before each measurement. To be able to optically image and record the areas investigated a camera was attached to the bright field microscope. The NicPlan infrared microscope used in these experiments was equipped with a 32× Cassegrain objective that could be used in two modes: view and collect. The sample-slides were placed under the microscope (at 320× magnification) and in the view mode, single cyanobacterial filaments or separated sheaths were located and centered near the desired position (Fig. 2) using a computer-controlled x-y stage. In addition, a spot free of sample was located and recorded (e.g., point marked 'B' in Fig. 2) to establish the background signal. The FTIR radiation is directed onto the sample for infrared analyses in the collect mode. In this study, per sample, at least three points on a cyanobacterial filament, and three on a separated sheath were identified for analysis. On each point, triplicate measurements were carried out with a sample-free background spectrum collected after every third measurement. Each spectrum was thus corrected for instrumental response and beam

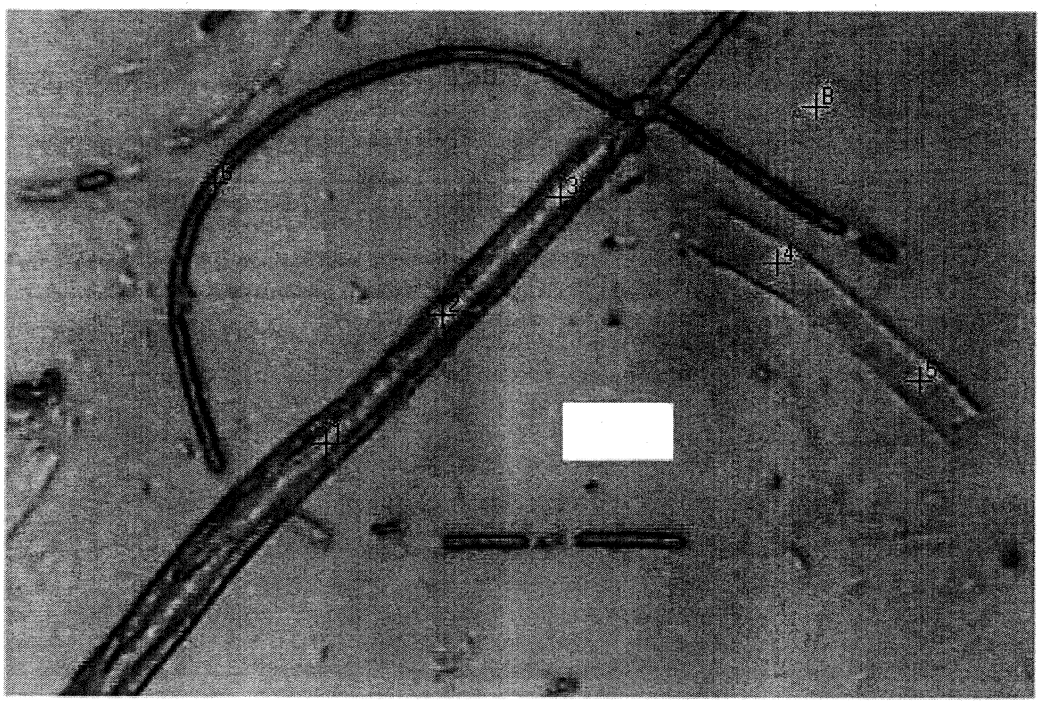

Fig. 2. Infrared bright field photomicrograph of a *Calothrix* sp. whole cell (points 1, 2, 3) and its separated sheath (points 4 and 5). The picture was captured in visible light mode at 320× magnification. The size of the white aperture 'box' is 20 × 10 μm^2 and B is the point where the background was measured. Note point 6, on a smaller bacterial filament (left upper corner), which denotes a point that was not used in the measurements because its size was smaller than the cutoff size set for all measurements (>90% of a 20 × 10 μm^2 aperture 'box' must be filled with sample).

profile by referencing against a background spectrum collected from a clear area of the IR reflecting slide.

Reflectance spectra over the range of 600 to 4000 cm^{-1} were collected with the aperture on the microscope set so that the beam was focussed onto a 20 × 10 μm^2 area. This allowed a high spatial resolution and the chosen aperture covered an area just slightly larger than the cyanobacterial filaments or the separated sheath material (Fig. 2). However, this aperture setting strongly affected the quality of the spectra below ~700 cm^{-1}. Decreasing the aperture dimension leads to a degradation of signal to noise ratio and, more importantly, as the aperture size approaches the wavelength of the infrared light diffraction becomes a problem. The diffraction limited spatial resolution is defined as (0.61 λ/NA), where λ is the wavelength of the energy and *NA* is the numerical aperture of the optical system (in this case $NA = 0.65$, Messerschmidt, 1995), and thus the lower limit for the aperture in all experiments was 20 × 10 μm^2. Only with such an aperture could a good signal to noise ratio be achieved and good quality data in the region of interest (vibrations at and below 1000 cm^{-1}) be acquired. Thus for each measurement, single filaments or sheaths that were similar in size (diameter ~8–10 μm) were chosen. This size was a prerequisite as multiple tests had shown that the best and most reproducible spectra were obtained when the cutoff size in the preset 20 × 10 μm^2 aperture 'box' was such that > 90% (±5%) of the 'box' was filled with sample. This was done to minimize variations due to sample thickness and water content.

4. RESULTS AND DISCUSSION

4.1. Vibrational Characteristics

4.1.1. Spectral Analysis and Corrections

The collected reflectance spectra were transformed into absorbance spectra ($A = \log[1/R]$) using the Nicolet OMNIC and Atlμs software (ThermoNicolet Ltd.) and are presented as absorbance vs. wavenumber (cm^{-1}). To derive the characteristic frequencies and to compare relative intensities, all background-corrected spectra were baseline corrected with the baseline set as a two-point straight-line between two end-points of a desired frequency region. This was done using the automatic baseline correction algorithm within the OMNIC software, either for 4000 to 700 cm^{-1} or for 1800 to 700 cm^{-1}. This procedure allowed a minimization of the differences between spectra due to baseline shifts and corrected for the intensity decay of the synchrotron beam. Furthermore, all baseline corrected silicified sample spectra were compared with the baseline corrected reference spectra to determine the quality of the baseline corrections and the changes in assigned peak position.

4.1.2. Spectral Reproducibility

A comparison of the raw, background corrected spectra of triplicate measurements on the same spot shows a high degree of reproducibility as indicated by the consistency between the relative peak intensities (<2.5% variation, five triplicate measurements). In addition, a comparison between relative intensities of spectra collected on two different points on the same filament (seven different samples) exhibit a variation in relative intensities of < 8% (Fig. 3). This variability may be caused by some degree of incomplete baseline correction but in part, it will be a consequence of the variations in sample thickness and non-uniformity of the deposited cells. Such differences can lead to variations in scattering and diffraction, which occur as the beam is refracted off the reflective slide. However, in this study

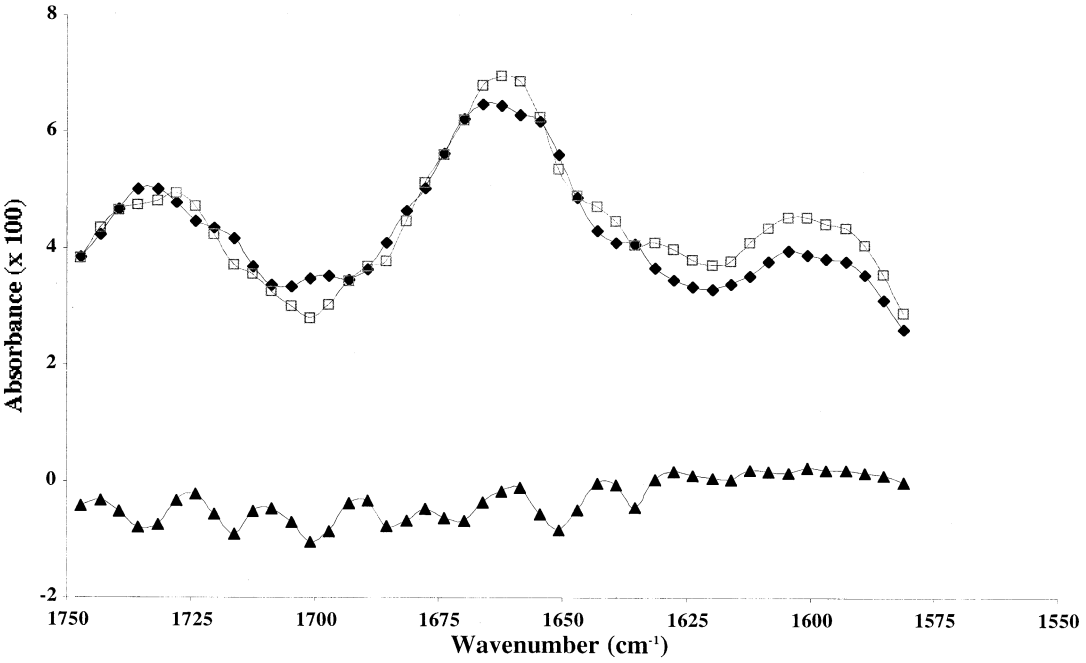

Fig. 3. Comparison between two spectra measured on the same *Calothrix* sp. filament but on different points, in order to assess the differences due to baseline correction, sample thickness variations and hydration levels. Points 1 (diamonds) and 2 (squares) were located ~30 μm apart from each other. The difference spectrum (triangles) is calculated using the standard subtraction function in OMNIC.

extreme care was taken to minimize these problems by selecting filaments and separated sheaths that were similar in size and appearance, and visibly free of loose particles.

4.1.3. Band Assignments: Calothrix sp. Whole-Cell and Purified Sheath Control Samples

To determine the main frequencies in the reference materials, spectra for a whole-cell control (unsilicified *Calothrix* sp.), a sheath control (unsilicified, chemically purified *Calothrix* sp. sheath) and a 10.7 mmol/L standard silica solution were compared and cross-referenced against literature data for microorganisms, macromolecules as well as aqueous and amorphous silica (see below and sources in Table 1). Although at high wavenumbers (>2000 cm^{-1}) some lipid, water and silica vibrations are found (bands 1–3 in Table 1; Figs. 4a and 4b), the most characteristic spectral features of cyanobacterial cellular components are observed between 700 and 1800 cm^{-1} (bands 4–14 in Table 1, Fig. 4d). Below 2000 cm^{-1}, two spectral regions have been distinguished: the "double bond" region (2000–1500 cm^{-1}, C=O bonds) and the "fingerprint" region (1500–600 cm^{-1}; Diem, 1993; Stuart and Ando, 1997).

4.1.3.1. Proteins. In the double bond region (2000–1500 cm^{-1}), dominantly in the whole-cell and less so in the chemically purified sheath, the protein spectra exhibit two primary features that arise from specific stretching and bending vibrations of the peptide backbone. The whole-cell spectra are dominated by the amide I feature at ~1650 cm^{-1} (band # 5, Figs. 4a and 4d). This band is sensitive to the protein's secondary structure, to ligand interactions and to its folding characteristics (Brandenburg and Seydel, 1996; Zeroual et al., 1995; Panick and Winter, 2000). The amide II vibration can be found at ~1540 cm^{-1} (band # 7) and consists mainly of a C-N stretching vibration coupled with an N-H bending vibration. In the chemically purified sheath the amide I and II bands are weaker and the amide II band has shifted to lower frequencies as a consequence of thermal denaturation due to the preparation procedure (see section 3.1). These two vibrations are usually the most characteristic features in a microbial spectrum but often an additional protein feature may be found at lower wavenumbers (e.g., amide III at ~1450 cm^{-1}; band # 8, Diem, 1993; Fig. 4a). However, in cyanobacterial spectra strong polysaccharide vibrations usually conceal the amide III vibrations.

4.1.3.2. Nucleic acids. The most distinctive absorption band for the nucleic acids can be found at ~1240 cm^{-1} (band # 10; Fig. 4a) and this band corresponds to the asymmetric phosphodiester stretching vibration (ν_{as}P=O) of the DNA or RNA backbone structure (Naumann et al., 1996). Another important nucleic acid phosphodiester peak is the symmetric stretching vibration at 1080 cm^{-1}, but in cyanobacteria, the main carbohydrate vibrations (see below) conceal this band.

4.1.3.3. Lipids. Below 2000 cm^{-1}, the main lipid band can be found at ~1740 cm^{-1} (>C=O ester stretching vibrations, band # 4), and is derived primarily from the ester linkage of the fatty acids (aliphatic monocarboxylic acids). This lipid feature can reach a maximum of 5 to 10% of the amplitude of the amide I

Table 1. Frequencies and band assignments for FTIR spectra derived from the *Calothrix* sp. whole-cells, purified sheath and silica spectra.

Band #	Wavenumbers (cm^{-1})	Assignments[a]	Main group with source[b]	Comment
1	~3750	Si_8O-H	Silica[22]	Surface hydroxyl groups
2	~3300–3400	v O-H and v N-H	Water[4,20]	Water/amide A;
3	~2960	v_{as} CH_3	Lipids[5]	Methyl groups
3	~2930	v_{as} CH_2	Lipids[5]	Methylene groups
3	~2875	v_s $>CH_2/-CH_3$	Lipids[4,5]	Methyl and methylene groups in fatty acids
4	~1740	v $>C=O$ of esters	Membrane lipids[1–5]	Fatty acids
4	~1710	v $>C=O$ of esters	Carboxylic group	Esters
5	~1650[c]	v C=O	Amide I[1–8]	Protein (mostly β-helical structure; the secondary structure of the protein can affect the position; 1695–1637 cm^{-1}[4])
6	~1630	v O-H	Water[17]	Water; for hydrated silica this represents the water in hydrogen-bonded silanols
7	~1540[c]	δ N-H and v C-N	Amide II[11–8]	Protein
8	~1450	δ_{as} CH_2 / δ_{as} CH_3	Lipid/amide III[2,5,8,10]	Broad methylene peaks with positions varying in the literature; amide III protein
9	~1392	v_s C-O	Carboxylic acids[2,8]	Stretching of carboxylates; can interfere with the methyl bending δ_s CH_2/δ_s CH_3 of the proteins and with the methyl bending, δ_s $N(CH_3)_3$ of the lipids
10	~1240[c]	v_{as} P=O	Nucleic acid[2,8–10]/ phosphoryl group	Stretching of phosphodiester backbone of the nucleic acids (DNA and RNA); general phosphoryl groups
11	~1200–950[c]	v C-O/v_{as} P=O ~1080 cm^{-1} for P=O ~1165, 1110, 1050 and 1030 for C-O	Polysaccharides[2,4,9]/ nucleic acid[8,9]	Dominated by the ring vibrations in polysaccharides; overlaps with stretching phosphodiester backbone of the nucleic acids (DNA and RNA); in the presence of silica these bands may be concealed by the stronger ionic siloxane band
12	~1150–1000[c]	v C-O / v Si-O 1190, 1060 cm^{-1} for Si-O	Polysaccharides [2,9] siloxane[11–15]	Main region for carbohydrate peaks; however, stretching of siloxanes interferes strongly with the stretching of carbohydrates; often exhibits a shoulder at ~1200 cm^{-1} that corresponds to the Si-O stretching vibrations of SiO_4 tetrahedra[15]
13	~950[c]	v Si-H_n (n = 1–3) v Si-OH	Silane/silanol[19,21]	Typical silica band on the shoulder of the main Si-O peak; usually of low amplitude; attributed to Si-O vibrations for silica glasses with non-bridging oxygens[18], or to the stretching mode of the Si-O (OH) bonds[19] in silica gels
14	~800[c]	v Si-O	Siloxane[18,20]/SiO_4 ring structure[16]	Corresponds to multiple siloxane bond (Si-O-Si) or chain ($Si_3O_9^{6-}$) vibrations in solid amorphous silica; sometimes interferes with silanol Si-OH stretching in silica gels

[c] Bands discussed in spectral evaluations. [a] v = stretching; δ = bending; as = asymmetric, s = symmetric [b] 1: Hendrick et al. (1991); 2: Zeroual et al. (1995); 3: Williams and Fleming (1996); 4: Nauman et al. (1996); 5: Stuart and Ando (1997); 6: Lewis and McElhancy (1996); 7: Giordano et al. (2001); 8: Nelson (1991); 9: Wong et al. (1991); 10: Liquier and Taillandier (1996); 11: Pouchard (1985); 12: Bertoluzza et al. (1982); 13: Padmaja et al. (2001); 14: Kloprogge et al. (2000); 15: Lazarev(1972); 16: Lippencot et al. (1958); 17: Socrates (2001); 18: Mukherjee (1980); 19: Zarzycki and Naudin (1962); 20: Keller (1986); 21: Nakamoto (1986); 21: Tripp and Hair (1991).

intensity and when the aliphatic lipids are conjugated with aromatic ring compounds this feature is often shifted to lower frequencies (~1730–1720 cm^{-1}, Keller, 1986). Other lipid vibrations can be found at ~1450 cm^{-1} (see above) and between 2900 and 3000 cm^{-1}, where three phospholipid vibrations are found (band # 3, Fig. 4a). These distinctive bands at ~2960, ~2930, and ~2875 cm^{-1} correspond to the symmetric and asymmetric vibrations of CH_2 methyl and CH_3 methylene groups.

4.1.3.4. Polysaccharides. The control samples for the *Calothrix* sp. whole-cells and purified sheaths both contain prominent features corresponding to complex carbohydrates (Figs. 4a and 4b). These features exhibited characteristic C-O derived carbohydrate absorption bands that spread over ~300 wavenumbers between 1200 and 900 cm^{-1} (bands covered by the regions # 11 and 12; Fig. 4). For *Calothrix* sp., the carbohydrate bands are the main distinguishing features in the 'fingerprint' region, since *Calothrix* sp. cells possess an ample polysaccharide sheath surrounding the cell body (Fig. 2; Weckesser et al., 1988; Phoenix et al., 2002). Carbohydrate peaks were found in both the whole-cell and the chemically purified sheath (at ~1165, ~1110, ~1050 and ~1030 cm^{-1}), but the frequency, position, and intensity could be established more accurately in the purified sheath spectra (Figs. 4b and 4d).

In the spectra for the chemically purified sheath control (Figs. 4b and 4d), at wavenumbers between 700 and 950 cm^{-1}, some additional weak bands were observed, (i.e., at ~820 cm^{-1} and a shoulder at ~900 cm^{-1}). However, these features could not be quantified in the silicified samples because the bands were weak and were obscured by the much stronger silica band (at ~800 cm^{-1}).

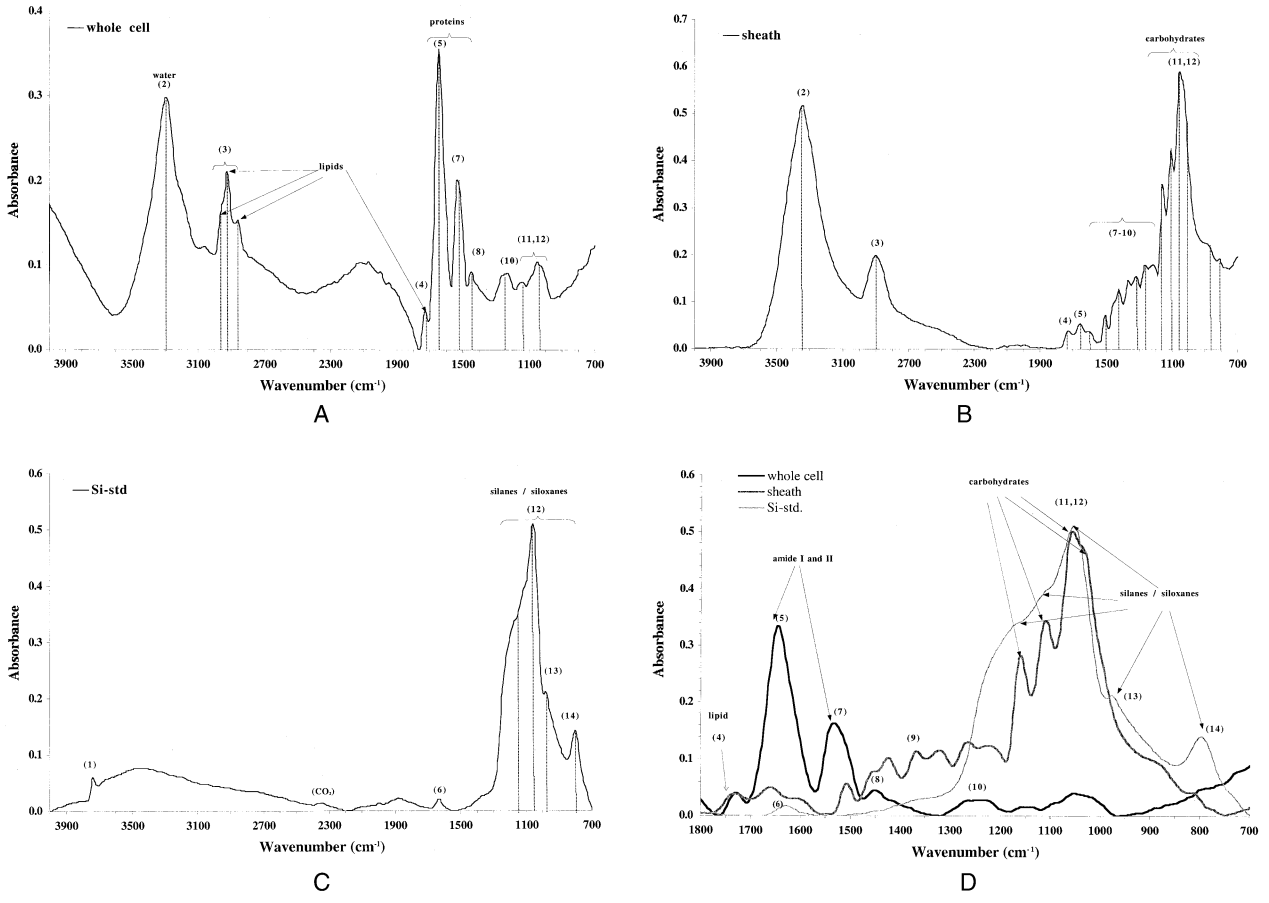

Fig. 4. Representative FTIR absorbance spectra for the reference materials: (a) *Calothrix* sp. whole-cell, (b) *Calothrix* sp. sheath, and (c) silica standard. All spectra were baseline corrected for wavenumbers between 4000 and 600 cm^{-1} and the details for the band assignments are discussed in Table 1 and in the text. (d) Enlargement of the "double bond and fingerprint region" for the standards shown in (a) to (c); main bands are indicated by dotted lines and numbers in brackets above the spectra correspond to the band # in Table 1.

4.1.4. Band Assignments: Silica, H_2O, and CO_2

For silica, the main absorption bands were derived by comparisons with literature values reported for silica gels, glasses, and amorphous silica powders (Fig. 4c; Table 1). The spectrum of the silica standard contains a peak at ~3750 cm^{-1} (band # 1), which indicates the presence of free silanols and is assigned to the isolated surface Si_8O-H groups (Tripp and Hair, 1991). Partly hydrated silica exhibits a band at ~1630 cm^{-1} (band # 6), which correspond to the stretching vibrations of adsorbed OH groups representing the hydrogen-bonded silanols with some water (Ringwald and Pemberton, 2000, band # 6). The presence of this band in the standard spectra shows that the silica is not fully dehydrated. It is worth noting that in a silicified cyanobacterial cell, other organic groups (i.e., amide I, and lipids) usually completely conceal this band. The main siloxane frequencies are found between 1200 and 800 cm^{-1} (bands # 12–14) and they partially overlap with the carbohydrate bands. The asymmetric Si-O stretching vibrations at 1190 and 1060 cm^{-1} are derived from the vibrations of SiO_4 tetrahedra with three or four bridged oxygens (Lazarev, 1972; Farmer, 1974). Usually, the bands for the Si-O group have a stronger ionic character and are therefore more intense than the corresponding carbohydrate C-O bands (Nakamoto, 1986). In many cases, a weak band at ~1115 cm^{-1} is manifested as a shoulder on the broad 1060 cm^{-1} peak (Figs. 4c and 4d; Farmer, 1974). This latter band however, strongly overlaps with the C-O bands of the carbohydrates (at 1050 cm^{-1}).

Fortunately, at lower frequencies two additional vibrations (950 and 800 cm^{-1}) typical for freshly precipitated silica gels are found (see Table 1 and Farmer, 1974). A medium intensity band at ~950 cm^{-1} (band # 13) can be assigned to the Si-O stretching of Si-OH silane and silanol groups in silica gels (Zarzycki and Naudin, 1962; Hino and Sato, 1971). This band can also represent the vibration of the Si-O bond in glasses or gels containing non-bridging oxygens (Moenke, 1966; Mukherjee, 1980). Furthermore, Moenke (1966) has shown that this band is a common feature in spectra for diatoms or opaline silica and that the 950 cm^{-1} band weakens and shifts to ~970 cm^{-1} as the Si-OH groups condense to form Si-O-Si bonds.

The 800-cm^{-1} band (band # 14) is assigned to the Si-O stretching vibrations of the SiO_4 ring structure. This is usually correlated with fully condensed Si atoms surrounded by four Si-O-Si linkages (Landmesser et al., 1997). Overall, amorphous silica structures, in contrast to their crystalline analogues, ex-

hibit no long-range order and are built up from SiO_4 tetrahedra with variable Si-O-Si bond angles and Si-O bond distances. These structures may comprise a large number of tetrahedrally coordinated silica atoms that are connected through oxygen atoms to other silicon atoms or to hydrogen atoms. Three or five coordinated silicon species are not expected to be stable in such structures (Perry, 1989). The centers of such a structure (gel or particle) are usually built up from chain or rings of various sizes and can essentially be fully dehydrated. However, the outside of such a particle will show a range of hydroxyl functionality and the hydration states will vary dramatically depending on the stage in the condensation process (Iler, 1981). Amorphous silica structures are usually formed by oligomerizing orthosilicic acid via the expulsion of water, which ultimately produces nanoparticles which grow to yield silica sols, gels or aggregates (Iler, 1981). In the infrared spectra presented here, these two bands (950 and 800 cm^{-1}) represent exclusive silica vibrations and for the 800-cm^{-1} band no interference with cyanobacterial cells, sheath vibrations or other silica bands were observed. For the 950-cm^{-1} Si-OH band, the only interference has been observed with the strong Si-O band at 1060 cm^{-1}. This strong Si-O band may cause the Si-OH band to weaken move to higher frequencies and become a shoulder of the 1050-cm^{-1} band (Moenke, 1966).

In all spectra (Figs. 4a–4c) liquid or gaseous water (at ~3500–3300 cm^{-1} band # 2), and gaseous CO_2 (at ~2360 cm^{-1}, band not listed in Table 1, but shown in Fig. 4c) are often present. They are IR active and the samples, although dried for 4 h, retained water in the cell structure and in the sheath, and CO_2 is present in the air. However, the amount of water in a sample depends on the size of the bacterial cell, on the covered area during measurement, on the dryness of the sample and on the amount of water vapour in the room. In all experiments, single bacterial filaments were measured and the same aperture used. In addition, all samples were dried in the same way and thus it was assumed that the amount of water in the samples was fairly constant. The number of people breathing close to the interferometer also affects the size of the CO_2 peaks. Although some studies have corrected for these features by subtracting standard H_2O or CO_2 spectra acquired using attenuated total reflectance (ATR) infrared standard spectra, water and CO_2 were not quantified by the methods used here, and thus no correction for H_2O or CO_2 was made. This correction was not necessary, as the vibrations affected by water and CO_2 (mostly lipids at high wavenumbers) were not used as characteristic bands in this study.

Thus, the whole-cell spectrum shows a combination of protein, lipid, and carbohydrate bands, and the sheath spectrum shows mainly polysaccharide bands. The characteristic bands for amorphous silica structures in part overlap with the carbohydrate bands but also show a distinctive band at ~800 cm^{-1}.

4.2. Silicification Experiments

After having identified the main vibrational features in the whole-cells and purified sheath controls, the progressively silicified *Calothrix* sp. samples were characterized via the changes in specific intensity and position of each band with increasing silica load. The measurements were carried out on single cyanobacterial filaments and on separated sheaths from each microcosm. Care was always taken to choose single filaments or separated sheaths (which were well separated from the other filaments, Fig. 2 that were of equal dimensions and appearance and free of loose particles.

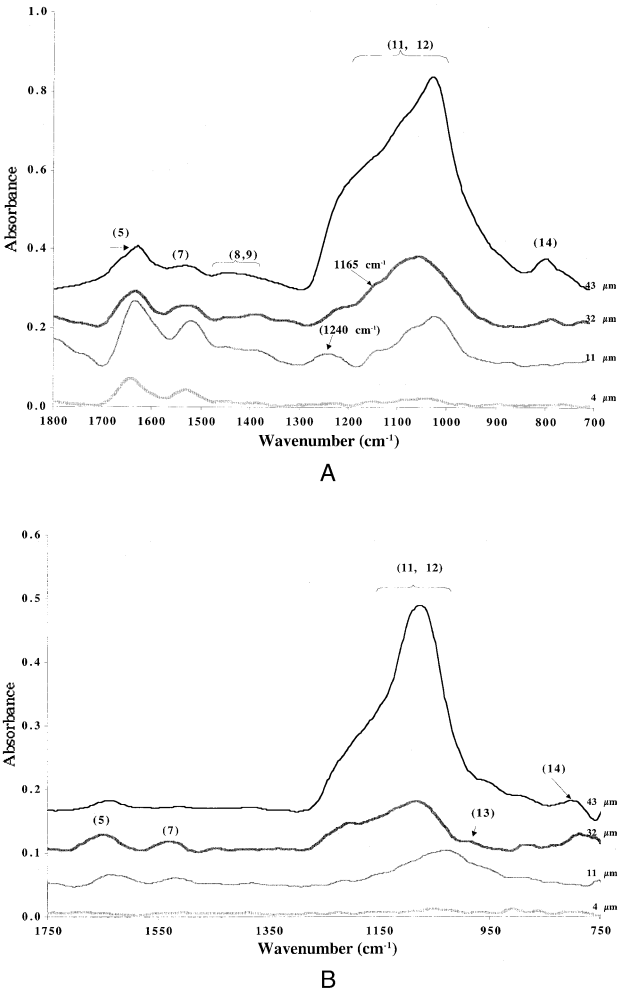

Fig. 5. Infrared absorbance spectra of the silicified *Calothrix* sp. filaments, plotted as a function of increasing silica-load (in μmol). All spectra were baseline corrected between 1800 and 700 cm^{-1}. (a) Whole-cell spectra, (b) spectra for the sheath; numbers to the right of the spectra correspond to silica load in micromoles while numbers in brackets above the spectra correspond to band # in Table 1. Infrared spectra have been vertically shifted for clarity.

4.2.1. Whole-Cells

The changes in the main spectral features during the progressive silicification of whole-cell samples are shown in Figure 5a. With increasing silicification (here shown as total sorbed Si in μmol) a ~90% increase in the intensity between 1250 and 950 cm^{-1} and the formation of a new band at ~800 cm^{-1} (band # 14) was observed. Some additional, less prominent changes in the features in this region need to be pointed out. Firstly, with increasing Si load (in micromoles sorbed Si) a shift in the amide I frequency towards lower wavenumbers occurred (~20–30 wavenumbers; horizontal arrow at band # 5 in Fig. 5a). The reason for this shift is unclear but with increas-

ing silicification protein denaturation (not thermal but chemical) may lead to this shift. Furthermore, the carboxylic acid and amide III bands (1392 and 1450 cm^{-1}, bands # 8 and 9) broadened and this latter change can be attributed to the more amplified Si-O and C-O vibrations around 1100 cm^{-1}. At roughly the same rate the increase in absorbance for the main Si-O/C-O region (1060–1030 cm^{-1}) causes the phosphodiester band (the P=O stretching band # 10, 1240 cm^{-1}) and the C-O band at 1165 cm^{-1} to transform into a shoulder of the main Si-O/C-O region.

The vibration bands corresponding to the frequencies at ~1100 to 1000 cm^{-1} were attributed to a mixture of the asymmetric Si-O stretching vibrations (intertetrahedral mode), and the carbohydrate C-O vibrations. The Si-OH band at 950 cm^{-1} is concealed in the whole-cell spectra (Fig. 5a) and is manifested only as a weak shoulder of the mixed Si-O/C-O region although when compared with the silica standard spectrum (Fig. 4c) this band is expected to form at the highest silica loads. However, the intense Si-O bands with stronger ionic character at 1050 cm^{-1} obscured this weaker Si-OH band. In many silica gels and opaline silicas this band is known to weaken, broaden and move to higher wavenumbers (970 cm^{-1}, Moenke, 1966) upon condensation and dehydroxylation of the silanol, Si-OH groups on the path to form Si-O-Si siloxane bridges (Farmer, 1974). Furthermore, in the whole-cell spectra the absorbance intensity value for the 1100- to 1000-cm^{-1} bands is ~5 times larger than the same band in the whole-cell control spectra (0.1 vs. 0.5). This dramatic increase will naturally affect all vibrational bands in the close surrounding (i.e., 1392, 1165 and 950 cm^{-1}).

However, the newly forming vibration at ~800 cm^{-1} corresponds exclusively to symmetric intratetrahedral Si-O stretching modes (Landmesser et al., 1997) and no interference with the carbohydrate or silica bands was observed. This band can thus be used to infer the formation of amorphous silica gel-like structures that are linked to the cyanobacterial cells. Mechanistically the formation of the 800-cm^{-1} band indicates the formation of stable Si-O-Si bonds via dehydroxylation of linked $Si(OH)_4$ tetrahedral units. This process has been attributed to pore closure in the gel-like nanocrystalline porous material followed by the collapse of the interconnected channels (Landmesser et al., 1997).

Scanning and transmission electron microscopic evidence (Phoenix et al., 2001; Benning et al., 2002, 2003) showed that during the silicification experiments silica particles accumulate on *Calothrix* sp. whole cells only extracelullarly, while intracellular silicification occurs only upon lysis of the cells. This however, is not the case here as in all whole-cell spectra we still see the prominent protein peaks attesting to the viability of the cells. Furthermore, Phoenix et al. (2000) showed that cells remain viable during biomineralization.

4.2.2. Separated Sheaths

Subsequent to the whole-cell measurements and at the same silica loads, spectra of mechanically separated cyanobacterial sheath fragments (see Fig. 2, and section 3.2.1) were recorded (Fig. 5b). The relative reflectance intensity of the sheaths was much lower than that for the whole-cells (~30–50% of whole-cell). This was mainly due to the fact that the sheaths that were separated from their original whole-cells were much thinner (at best two layers of ~0.02–0.5 μm, vs. up to 5-μm-thick whole-cells; Weckesser et al., 1988; Shi et al., 1995, Phoenix, 2001).

With increasing silica load, similar to the whole-cells, the absorbance intensity for the C-O and Si-O bands in the separated sheath spectra (bands in region # 11, 12) increased steadily (by ~75%). In addition, at the highest silica loads (32 and 43 μmol), both exclusive silica bands clearly emerged (at ~950 cm^{-1}, band # 13 and at ~800 cm^{-1}, band # 14). In the silicified sheath spectra the 950-cm^{-1} band was clearly observed (Fig. 5b), while this band was mostly concealed in the whole-cell spectra (Fig. 5a). The reason for this difference is unclear, but could stem from the much higher absorbance intensity of the Si-O bands at ~1000 to 1100 cm^{-1} the silicified whole-cell spectra (up to 50% higher than in the separated sheath).

4.2.3. Silicification Synopsis

The spectra demonstrate that in both cases, in the *Calothrix* sp. whole-cell and in the sheath, the intensity of the bands between 750 and 1300 cm^{-1} increased considerably with increasing silica load. The vibrations in this region correlate with the formation of polysaccharide and, at the highest silica loads, the formation of silica related bonds. These bonds were observed in the silicified whole-cells but also in the silicified sheaths. This suggests that the reaction between the live cell and the silica solution occurred predominantly on the surface of the sheath although the cell wall itself is considered by far the more reactive surface (i.e., the sheath contains only ~15% of the total reactive functional groups on the surface of *Calothrix* sp., and most functional groups are located upon the cell wall; Phoenix et al., 2002). Note that during the progressive silicification, the sheaths still enclosed the filaments and that the mechanical separation of sheath from the filament only occurred before FTIR measurements, during the sonication step (see section 3.2.1).

Microorganisms such as *Calothrix* sp. produce an extracellular polysaccharide (EPS) coating for a number of reasons, including protection against predation and dehydration (Dudman, 1977; Scott et al., 1996; Hoiczyk, 1998; Wilson et al., 2001), prevention of detrimental biomineralization (Phoenix et al., 2000), and to aid adhesion to a substrate (Dudman, 1977; Scott et al., 1996). In both the whole-cell and the separated sheath the increase in spectral intensity of the silica and carbohydrate bands was interpreted as a combination of increase in EPS sheath thickness followed by the silicification of the bacterial filaments in response to the amorphous silica precipitation.

These results corroborate the work by Phoenix et al. (2000), who suggested that the sheath may be necessary to provide the means for photosynthetically active cyanobacteria to survive mineralization. This process might be assisted by the sheath acting as the mineral deposition site, thus provide a physical barrier against colloidal silica deposition and thus preventing cell wall and/or cytoplasmic mineralization. This may also explains why the observed silicification of the sheath predominates over cell silicification. This is however, the first time that this process has been monitored in situ on live cells.

The thickness of the sheath when attached to the cell grows

in response to the silicification, but at some point, the sheath C-O vibrational frequencies cease to dominate and the more ionic linked Si-O bonds control the spectrum. However, it is clear that the cellular substrates are still important and that silica does not exclusively govern the spectra, because the characteristic protein (at ~1650 cm^{-1}, Fig. 5a) and lipid bands (at ~2900 cm^{-1}, data not shown) are still present. In addition, microscopic SEM/TEM evidence (Phoenix, 2001, Phoenix et al., 2001; Benning et al., 2003), also endorse the argument that the sheath thickens in response to amorphous silica deposition.

5. CONCLUSIONS

The goal of this study was to establish the vibrational frequencies corresponding to the organic functional groups of cyanobacterial cells and cell components and to ascertain the change in these frequencies during silicification. This was the basis for determining whether microorganisms play an active role in biomineralization and how they respond to biomineralization. In this study we have (1) demonstrated that reactions occurring between organic biomolecules on microbial surfaces and silica solutions can be monitored in situ; (2) determined the structure of cyanobacterial biomolecules and silica precipitates and (3) determined the changes in vibrational frequencies caused by the interaction of silica with the main compounds of live *Calothrix* sp. cells. The molecular level changes observed during the progressive deposition of amorphous silica on the sheath, when combined with other microscopic observations, improve our understanding of the mechanisms and processes that occur in environments where cyanobacteria play a crucial role in regulating the changes in their chemical environment.

The sequence of events observed in the silicified whole-cells and in the silicified mechanically separated sheaths suggests that, with increasing Si load initially, an increase in carbohydrate (absorbance increase in the mixed C-O/Si-O region) but no formation of independent Si-O bonds at 800 cm^{-1} was observed. However, the formation of independent silica units on the cell and sheath surface was observed at the highest silica loads (32 and 43 μmol sorbed Si). This leads us to postulate that during silicification a mechanistic switch is occurring. Initially, the process is governed by a mechanism controlled by growth of sheath in response to silicification and possible hydrogen bonding of the silica to the sheath. At higher Si loads a switch to a mechanism controlled by a fully abiotic process leading to the full silicification of the cells is postulated. The quantification of the dynamics of the silicification based on the changes in infrared spectral characteristics is presented elsewhere (Benning et al., 2003).

The experimental evidence presented above shows that cyanobacteria interact actively with a polymerizing silica solution, and that this interaction can be monitored and quantified. Once the initial silica sorption stage is complete, the formed silica substrate will enhance the precipitation of amorphous silica via an autocatalytic, abiogenic growth process thus permitting the formation of silica encrusted microorganisms as observed in many hot spring environments (e.g., Beveridge and Murray, 1980; Ferris et al., 1986; Urrutia and Beveridge, 1994; Jones et al., 2001; Konhauser et al., 2001; Phoenix et al., 2001; Mountain et al., 2002).

Acknowledgments—The financial support provided by the UK Natural Environment Research Council, Direct Access to Synchrotron Radiation Source grant (#37059) and by a grant from The Leverhulme Thrust (Ref. #F/00122/F) are greatly acknowledged. V. Phoenix at the University of Toronto was kindly supported by Professor F. Grant Ferris though The Natural Science and Engineering Research Council (NSERC) of Canada, and through an Ontario Premier's Research Excellence Award. The reviews of Anne Hofmeister, Sherry Cady and a third anonymous reviewer were much appreciated, as their comments and suggestion much improved this paper.

Associate editor: J. P. Amend

REFERENCES

Awramik S. M. (1992) The oldest records of photosynthesis. *Photosyn. Res.* **33,** 75–89.

Benning L. G., Phoenix V., Yee N., Tobin M. J., Konhauser K. O., and Mountain B. W. (2002) Molecular characterization of cyanobacterial cells during silicification: A synchrotron-based infrared study. *Geochem. Earth Surf.* **6,** 259–263.

Benning L. G., Phoenix V., Yee N., and Konhauser K. O. (2003) The dynamics of cyanobacterial silicification: An infrared micro-spectroscopic investigation. *Geochim. Cosmochim. Acta* **67,** 0000–0000.

Bertoluzza A., Fagano C., Morelli M. A., Gottardi V., and Guglielni M. J. (1982) Raman and infrared spectra on silica gel evolving toward glass. *J. Non-Cryst. Solids* **48,** 117–128.

Beveridge T. J. and Murray R. G. E. (1980) Sites of metal deposition in the cell wall of *Bacillus subtilis*. *J. Bacteriol.* **141,** 876–887.

Brandenburg K. and Seydel U. (1996) Fourier transform infrared spectroscopy of cell surface polysaccharides. In *Infrared Spectroscopy of Biomolecules* (eds. H. H. Mantsch and D. Chapman), pp. 203–238. Wiley-Liss, New York.

Brock T. D., Madigan M. T., Martinko J. M., and Parker J. (1994) *Biology of Microorganisms* 7th ed. Prentice Hall, Englewood Cliffs, NJ.

Cady S. L. (2001) Paleobiology of the Archean. *Adv. Appl. Microbiol.* **50,** 3–35.

Carr G. L. (1999) High-resolution microspectroscopy and sub-nanosecond time-resolved spectroscopy with the synchrotron infrared source. *Vib. Spectrosc.* **19,** *1,* 53–60.

Carr G. L. (2001) Resolution limit for infrared microspectroscopy explored with synchrotron radiation. *Rev. Sci. Instrum.* **72,** *3,* 1613–1619.

Carroll S., Mroczek E., Alai M., and Ebert M. (1998) Amorphous silica precipitation (60 to 120 degrees C): Comparison of laboratory and field rates. *Geochim. Cosmochim. Acta* **62,** 1379–1396.

Chiriboga L., Yee H., and Diem M. (2000) Infrared spectroscopy of human cells and tissue. Part VI: A comparative study of histopathology and infrared microspectroscopy of normal, cirrhotic, and cancerous liver tissue. *Appl. Spectrosc.* **54,** *1,* 1–8.

Choo-Smith L. Q., Maquelin K., van Vreeswijk T., Bruining H. A., Puppels G. J., Thi N., Kirschner C., Naumann D., Ami D., Villa A. M., Orsini F., Doglia S. M., Lamfarraj H., and Sockalingum G. D. (2001) Investigating microbial (micro)colony heterogeneity by vibrational spectroscopy. *Appl. Environ. Microbiol.* **67,** *4,* 1461–1469.

Daughney C. J., Fein J. B., and Yee N. (1998) A comparison of the thermodynamics of metal adsorption onto two common bacteria. *Chem. Geol.* **144,** 161–176.

Diem M. (1993) *Introduction to Modern Vibrational Spectrscopy*. Wiley Interscience, New York.

Diem M., Boydston-White S., and Chiriboga L. (1999) Infrared spectroscopy of cells and tissues: Shining light onto a novel subject. *Appl. Spectrosc.* **53,** *4,* 148A–161A.

Dove P. M. and Crerar D. A. (1990) Kinetics of quartz dissolution in electrolyte-using a hydrothermal mixed flow reactor. *Geochim. Cosmochim. Acta* **54,** 955–969.

Drews G. and Weckesser J. (1982) Function, structure and composition of cell walls and external layers. In *The Biology of Cyanobacteria* (eds. N. G. Carr and B. A. Whitton), pp. 333–357. Blackwell Scientific Publications, Oxford, UK.

Dudman W. F. (1977) The role of surface polysaccharides in natural environments. In *Surface Carbohydrates of the Prokaryotic Cell* (ed. I. Sutherland), pp. 357–414. Academic Press, London.

Farmer V. C. (1974) The infrared spectra of minerals. *Min. Soc. Mon.* **4,** 360–370.

Fay P. (1983) The blue-greens (cyanophyta-cyanobacteria). In *Studies in Biology/Institute of Biology*, **160**. Edward Arnold Ltd., London.

Fein J. B., Scott S., and Rivera N. (2002) The effect of Fe on Si adsorption by Bacillus subtilis cell walls: Insights into non-metabolic bacterial precipitation of silicate minerals. *Chem. Geol.* **182,** 265–273.

Ferris F. G., Beveridge T. J., and Fyfe W. S. (1986) Iron-silica crystallite nucleation by bacteria in a geothermal sediment. *Nature* **320,** 609–611.

Ferris F. G., Fyfe W. S., and Beveridge T. J. (1988) Metallic ion binding by bacillus subtilis—Implications for the fossilization of microorganisms. *Geology* **16,** 149–152.

Fortin D., Ferris F. G., and Beveridge T. J. (1997) Surface mediated mineral development by bacteria. In *Geomicrobiology: Interactions Between Microbes and Minerals* (eds. J. F. Banfield and K. H. Nealson). Mineralogical Society of America, Washington DC.

Fournier R. O. (1985) The behaviour of silica in hydrothermal solutions In *Geology and Geochemistry of Epithermal Systems* (eds. B. R. Berger and P. M. Bethke), **2,** 45–61. Soc. Econ. Geol.

Giordano M., Kansiz M., Heraud P., Beardall J., Wood B., and McNaughton D. (2001) Fourier transform infrared spectroscopy as a novel tool to investigate changes in intracellular macromolecular pools in the marine microalga Chaetoceros muellerii (Bacillariophyceae). *J. Phycol.* **37,** 271–279.

Hino M. and Sato T. (1971) Infrared absorption spectra of silica gel-water, water-d_2, and water-^{18}O systems. *Bull. Chem. Soc. Jpn.* **44,** 33–37.

Henley R. W., Truesdell A. H., Barton P. B. and Whitney J. A. (1984) Fluid-mineral equilibria in hydrothermal systems. *Rev. Econ. Geol.* **1**. Soc. Econ. Geol.

Hoiczyk E. (1998) Structural and biochemical analysis of the sheath of Phormidium uncinatum. *J Bacteriol.* **180,** *5,* 3923–3932.

Holman H.-Y. N., Perry D. L., Martin M. C., Lamble G. M., McKinney W. R., and Hunter-Cevera J. C. (1999) Real-time characterization of biogeochemical reduction of Cr(VI) on basalt surfaces by SR-FTIR imaging. *Geomicrobiol. J.* **16,** *4,* 307–324.

Holman H.-Y. N., Goth-Goldstein R., Martin M. C., Russell M. L., and Mckinney W. R. (2000a) Low-dose responses to 2,3,7,8-tetrachlorodibenzo-p-dioxin in single living human cells measured by synchrotron infrared spectromicroscopy. *Environ. Sci. Technol.* **34,** 2513–2517.

Holman H.-Y. N., Martin M. C., Blakely E. A., Bjornstad K., and McKinney W. R. (2000b) IR spectroscopic characteristics of cell cycle and cell death probed by synchrotron radiation based Fourier transform IR spectromicroscopy. *Biopolymers* **57, (***6*), 329–335.

Holman H.-Y. N., Nieman K., Sorensen D. L., Miller C. D., Martin M. C., Borch T., McKinney W. R., and Sims R. C. (2002) Catalysis of PAH biodegradation by humic acid shown in synchrotron infrared studies. *Environ. Sci. Technol.* **36,** *6,* 1276–1280.

Iler R. K. (1981) *The Chemistry of Silica*. Plenum Press, New York.

Jamin N., Dumas P., Moncuit J., Fridman W., Teillaud J., Carr G. L., and Williams G. P. (1998a) Highly resolved chemical imaging of living cells by using synchrotron infrared microspectrometry. *Proc. Natl. Acad. Sci. U. S. A.* **95,** *9,* 4837–4840.

Jamin N., Dumas P., Moncuit J., Fridman W., Teillaud J., Carr G. L., and Williams G. P. (1998b) Chemical imaging of nucleic acids, proteins and lipids of a single living cell. Application of synchrotron infrared microspectrometry in cell biology. *Cell. Mol. Biol.* **44,** *1,* 9–13.

Jones B., Renaut R. W., and Rosen M. R. (2000) Stromatolites forming in acidic hot-spring waters, North Island, New Zealand. *Palaios* **15,** 450–475.

Jones B., Renaut R. W., and Rosen M. R. (2001) Taphonomy of silicified filamentous microbes in modern geothermal sinters—Implications for identification. *Palaios* **16,** 580–592.

Kansiz M., Heraud P., Wood B., Burden F., Beardall J., and McNaughton D. (1999) Fourier transform infrared microspectroscopy and chemometrics as a tool for the discrimination of cyanobacterial strains. *Phytochemistry* **52,** 407–417.

Keller R. J. (1986) *Sigma Library of FT-IR Spectra*. Sigma Chemical Company, St. Louis, MO.

Kloprogge J. T., Frost R. L., and Hickey L. (2000) Infrared emmision spectroscopic study of the dehydroxylation of some hectorites. *Thermochim. Acta* **345,** 145–156.

Konhauser K. O. and Ferris F. G. (1996) Diversity of iron and silica precipitation by microbial mats hydrothermal waters, Iceland: Implications for Precambrian iron formations. *Geology* **24,** 323–326.

Konhauser K. O., Phoenix V. R., Bottrell S. H., Adams D. G., and Head I. M. (2001) Microbial-silica interactions in Icelandic hot spring sinter: Possible analogues for some Precambrian siliceous stromatolites. *Sedimentology* **48,** 415–433.

Krumbein W. E. (1983) *Microbial Geochemistry*. Blackwell Scientific Publications, Oxford, UK.

Landmesser H., Kosslick H., Storek W., and Fricke R. (1997) Interior surface hydroxyl groups in ordered mesoporous silicates. *Solid State Ionics* **271,** 101–103.

Lasch P., Boese M., Pacifico A., and Diem M. (2002) A FT-IR spectroscopic investigations of single cells on the subcellular level. *Vib. Spectrosc.* **28,** *1,* 147–157.

Lazarev A. N. (1972) *Vibrational Spectra and Structure of Silicates*. Consultants Bureau, New York.

LeVine S. M. and Wetzel D. L. (1998) Chemical analysis of multiple sclerosis lesions by FT-IR microspectroscopy. *Free Rad. Biol. Med.* **25,** *1,* 33–41.

Lewis R. N. and McElhaney R. N. (1996) Fourier transform infrared spectroscopy in the study of hydrated lipids and lipid bilayer membranes. In *Infrared Spectroscopy of Biomolecules* (eds. H. H. Mantsch and D. Chapman), pp. 159–202. John Wiley, Chichester, UK.

Lippencot E. R., van Valkenburg A., Weir C. E., and Bunting E. N. (1958) Infrared studies of polymorphs of silica and germania. *J. Res. Nat. Bur. Stand.* **61,** 61–70.

Liquier J. and Taillandier E. (1996) Infrared spectroscopy of nucleic acids. In *Infrared Spectroscopy of Biomolecules* (eds. H. H. Mantsch and D. Chapman), pp. 131–158. John Wiley, Chichester, UK.

Lowenstam H. A. (1981) Minerals formed by organisms. *Science* **211,** 1126–1131.

Martin M. C., Tsvetkova N. M., Crowe J. H., and McKinney W. R. (2001) Negligible sample heating from synchrotron infrared beam. *Appl. Spectrosc.* **55,** *2,* 111–113.

Martin M. C., Holman H-Y. and McKinney W. R. (2002) First performance results for a new continuum IR microscope. *ALS IR News* **7**.

McMillan P. F. and Hofmeister A. M. (1988) Infrared and Raman spectroscopy. *In Rev. Mineral.* **18,** 99–160.

Messerschmidt R. G. (1995) Minimizing optical nonlinearities in infrared microspectroscopy. In *Practical Guide to Infrared Microspectroscopy*, Vol. 3 (ed. H. J. Humecki), Marcel Dekker, New York.

Miller L. M., Carlson C. S., Carr G. L., and Chance M. R. (1998) A method for examining the chemical basis for bone disease: Synchrotron infrared microspectroscopy. *Cell. Mol. Biol.* **44,** *1,* 117–127.

Miller L. M., Tague J. R., and Thomas J. (2002) Development and biomedical applications of fluorescence-assisted synchrotron infrared micro-spectroscopy. *Vib. Spectrosc.* **28,** *1,* 159–165.

Moenke H. (1966) *Mineralspektren II* [in German]. Akademie Verlag, Berlin, Germany.

Mountain B. W., Benning L. G., and Boerema J. (2002) Biomineralization in New Zealand geothermal areas: Rates of growth and trace metal incorporation. *Geochem. Earth Surf.* **6,** 276–282.

Mukherjee J. (1980) Sol-gel processes in glass science and technology. *J. Non-Cryst. Solids* **42,** 477–488.

Nakamoto K. (1986) *Infrared and Raman Spectra of Inorganic and Coordination Compounds*. John Wiley, New York.

Naumann D. (1997) FT-IR and FT-Raman spectroscopy in medical microbiology. In *Spectroscopy of Biological Molecules: Modern Trends* (eds. P. Carmona, R. Navarro, and A. Hernanz), pp. 433–434. Kluwer, Dordrecht, the Netherlands.

Naumann D. (2000) Infrared spectroscopy in microbiology. In *Encyclopedia of Analytical Chemistry* (ed. R. A. Meyers), pp. 102–131.

Naumann D., Helm D., and Labischinski H. (1991) Microbiological characterizations by FT-IR spectroscopy. *Nature* **351,** 81–82.

Naumann D., Schultz C., and Helm D. (1996) What can infrared spectroscopy tell us about the structure and composition of intact bacterial cells? In *Infrared Spectroscopy of Biomolecules* (eds. H. H. Mantsch and D. Chapman), pp. 279–310. Wiley-Liss, New York.

Nelson W. H. (1991) *Modern Techniques for Rapid Microbiological Analysis*. VCH, New York.

Padmaja P., Anilkumar G. M., Mukundan P., Aruldhas G., and Warrier K. G. K. (2001) Characterization of stoichiometric sol-gel mullite by fourier transform infrared spectroscopy. *Int. J. Inorg. Mat.* **3,** 693–698.

Panick G. and Winter R. (2000) Pressure-induced unfolding/refolding of ribonuclease A: Static and kinetic Fourier transform infrared spectroscopy study. *Biochemistry* **39,** *7*, 1862–1869.

Parker F. S. (1983) *Applications of Infrared, Raman, and Resonance Raman Spectroscopy in Biochemistry*. Plenum Press, New York.

Perry C. C. (1989) Biogenic silica. In *Biomineralisation, Chemical and Biological Perspectives* (eds. S. Mann, J. Webb, and R. J. P. Williams), pp. 233–256. VCH, Weinheim.

Phoenix V. R. (2001) *Microbial-Biomineral Interactions and Their Significance for the Formation of Chemical Sediments*. Ph.D. dissertation, University of Leeds.

Phoenix V. R., Adams D. G., and Konhauser K. O. (2000) Cyanobacterial viability during hydrothermal biomineralization. *Chem. Geol.* **169,** 329–338.

Phoenix V. R., Konhauser K. O., Adams D. G., and Bottrell S. H. (2001) Role of biomineralization as an ultraviolet shield: Implications for Archean life. *Geology* **29,** 823–826.

Phoenix V. R., Martinez R. E., Konhauser K. O., and Ferris F. G. (2002) Characterization and implications of the cell surface reactivity of the cyanobacteria Calothrix sp. (strain KC97). *Appl. Environ. Microbiol.* **68,** 4827–4834.

Phoenix V. R., Konhauser K. O. and Ferris F. G. (in press) Experimental study of iron and silica immobilization by bacteria in mixed Fe-Si systems: Implications for microbial silicification in hotsprings.

Pouchard C. J. (1985) *Aldrich Library of FT-IR Spectra, Vol. 2*. Aldrich Chemical Company Inc., Milwaukee, WI.

Reffner J. A., Martoglio P. A., and Williams G. P. (1995) FTIR microscopical analysis with synchrotron radiation: The microscope optics and system performance. *Rev. Sci. Instr.* **66,** 1298.

Rimstidt J. D. and Barnes H. L. (1980) The kinetics of silica-water reactions. *Geochim. Cosmochim. Acta* **44,** 1683–1699.

Ringwald S. C. and Pemberton J. E. (2000) Adsorption interactions of aromatics and heretoaromatics with hydrated and dehydrated silica surfaces by Raman and FTIR spectroscopies. *Environ. Sci. Technol.* **34,** 259–265.

Schultz C. and Naumann D. (1991) In vivo study of the state of order of the membranes of gram-negative bacteria by Fourier-transform infrared spectroscopy (FT-IR). *FEBS Lett.* **294,** 43–46.

Schultze-Lam S., Ferris F. G., Konhauser K. O., and Wiese R. G. (1995) In situ silicification of an Icelandic hot spring microbial mat: Implications for microfossil formation. *Can. J. Earth Sci.* **32,** 2021–2026.

Schuster K. C., Metrens F., and Gapes J. R. (1999) FTIR spectroscopy applied to bacterial cells as a novel method for monitoring complex biotechnological processes. *Vib. Spectrosc.* **19,** 467–477.

Scott C., Fletcher R. L., and Bremer G. B. (1996) Observations of the mechanisms of attachment of some marine fouling blue-green algae. *Biofouling* **10,** 161–173.

Shi L., Carmichael W. W., and Miller I. (1995) Immunogold localization of hepatotoxins in cyanobacterial cells. *Arch. Microbiol.* **163,** 7–15.

Sigee D. C., Dean A., Levado E., and Tobin M. J. (2002) Fourier-transform infrared spectroscopy of Pediastrum duplex: Characterization of micro-population isolated from a eutrophic lake. *Eur. J. Phycol.* **37,** 19–26.

Socrates G. (2001) *Infrared and Raman Characteristic Group Frequencies*: *Tables and Charts*. 3rd ed. John Wiley, Chichester, UK.

Stuart B. and Ando D. J. (1997) *Biological Applications of Infrared Spectroscopy*. John Wiley, Chichester, UK.

Tobin M. J., Chesters M. A., Pearson M., Griffin N. R., Fisher S. E., and Ruzicka B. (1999) Synchrotron IR microspectroscopy of malignant tissue. *Proc. SPIE Int. Soc. Opt. Eng., Soc. Phot-Opt. Instr. Eng.* **3775,** 96–103.

Tripp C. P. and Hair M. (199l) Reaction of chloromethylsilanes with silica: A low-frequency infrared study. *Langmuir* **7,** 923–927.

Urrutia M. M. and Beveridge T. J. (1994) Formation of fine-grained metal and silicate precipitates on a bacterial surface (Bacillus subtilis). *Chem. Geol.* **116,** 261–280.

Walter M. R., Bauld J., and Brock T. D. (1972) Siliceous algal and bacterial stromatolites in hot spring and geyser effluents of Yellowstone National Park. *Science* **178,** 402–405.

Ward D. M., Ferris M. J., Nold S. C., and Bateson M. M. (1998) A natural view of microbial biodiversity within hot spring cyanobacterial mat communities. *Microbiol. Mol. Biol. Rev.* **62,** 1353–1370.

Weckesser J., Hofmann K., Jürgens U. J., Whitton B. A., and Raffelsberger B. (1988) Isolation and chemical analysis of the sheaths of the filamentous cyanobacteria *Calothrix parienta* and *C. scopulorum*. *J. Gen. Microbiol.* **134,** 629–634.

Westall F., Boni L., and Guerzoni E. (1995) The experimental silicification of microorganisms. *Palaeontology* **38,** 495–528.

Wetzel D. L. and Levine S. M. (1999) Imaging molecular chemistry with infrared microscopy. *Science* **285,** 1224–1225.

Williams D. H. and Fleming I. (1996) *Spectroscopic Methods in Organic Chemistry*. 5th ed. McGraw-Hill International Ltd., London.

Wilson W. W., Wade M. M., Holman S. C., and Champlin F. R. (2001) Status of methods for assessing bacterial cell surface charge properties based on zeta potential measurements. *J. Microbiol. Meth.* **43,** 153–164.

Wong P. T. T., Wong R. H., Caputo T. A., Godwin T. A., and Rigas B. (1991) Infrared-spectroscopy if exfoliated human cervical cells—Evidence of extensive structural changes during carcinogenesis. *Proc. Natl. Acad. Sci. U. S. A.* **88,** 10988–10992.

Yee N., Phoenix V. R., Konhauser K. O., Benning L. G. and Ferris F. G. (2003) The effect of cyanobacteria on Si precipitation kinetics at neutral pH: Implications for bacterial silicification in geothermal hot springs. *Chem. Geol.* **99,** 83–90.

Zarzycki J. and Naudin F. (1962) Spectres infrarouges de la cristobalite et de quelques composes isostructuraux de SiO_2 comme GeO_2 ou BeF_2; etude comparative des reseaux vitreux. *Adv. Mol. Spectrosc.* **3,** 1071–1083.

Zeroual W., Manfait M., and Choisy C. (1995) FT-IR spectroscopy study of perturbations induced by antibiotic on bacteria. *Pathol. Biol.* **43,** *4*, 300–305.